



Calculation of Wakefields and Higher Order Modes for the Vacuum Chamber of the ATLAS Experiment for the HL-LHC

R. Wanzenberg and O. Zagorodnova
DESY, Notkestr. 85, 22603 Hamburg, Germany

Keywords: Wakefields, Higher Order Modes, ATLAS vacuum chamber, HL-LHC

Summary

A design study for a High Luminosity Large Hadron Collider (HL-LHC) was started to extend the discovery potential of the Large Hadron Collider (LHC). The HL-LHC study implies also an upgraded configuration of the ATLAS detector with a new beam pipe. The trapped Higher Order Modes (HOMs) and the short range wakefields for the new design of the vacuum chamber are calculated using the computer codes MAFIA and ECHO2D. The short range wakefields are characterized in terms of kick and loss parameters. For the HOMs the frequency the R/Q and the Q-values are given which can directly converted into impedance data. The obtained data are intended to be included into the impedance database of the HL-LHC.

The HiLumi LHC Design Study is included in the High Luminosity LHC project and is partly funded by the European Commission within the Framework Programme 7 Capacities Specific Programme, Grant Agreement 284404.

1 Introduction

1.1 The LHC accelerator

To extend the discovery potential of the LHC [1] a design study for a upgraded machine configuration, the High Luminosity LHC (HL-LHC), was started in 2011, with the goal to increase its peak luminosity (without levelling) by a factor of

7.4 beyond its design value. The HL-LHC study implies also an upgraded configuration of the ATLAS detector with a new beam pipe. Calculation of trapped Higher Order Modes (HOMs) and the short range wakefields for the new design of the vacuum chamber are presented in this report. A similiar study was already done for the vacuum chamber of the CMS experiment [2].

For the HL-LHC two options are considered, one with a bunch-to-bunch spacing of 50 ns and another one with 25 ns. The basic parameters of both options are presented in Table 1.

Parameter	Option 1	Option 2	
Proton energy	7	7	TeV
Ring circumference	26658.883	26658.883	m
Revolution frequency	11.245	11.245	kHz
Transverse normalized emittance	2.5	3.0	mm mrad
RMS bunch length	7.5	7.5	cm
Number of bunches	2808	1404	
Bunch spacing	25	50	ns
Number of particles per bunch	$2.2 \cdot 10^{11}$	$3.5 \cdot 10^{11}$	
Charge of one bunch	35.2	56.1	nC
Circulating beam current	1.11	0.89	A

Table 1: Two design parameters options under consideration for the HL-LHC.

It is also considered to use shorter bunches with an RMS bunch length of 4.0 cm. But for the wake field calculations it is assumed that the charge density is a Gaussian distribution with an RMS bunch length of $\sigma_z = 7.5$ cm:

$$\rho(z) = q_b g(z), \quad \text{with } g(z) = \frac{1}{\sigma_z} \frac{1}{\sqrt{2\pi}} \exp\left(-\frac{1}{2}\left(\frac{z}{\sigma_z}\right)^2\right). \quad (1)$$

The Gaussian function g is plotted in Fig. 1, while the Fourier transform of g and the spectral power density h , defined as

$$\tilde{g}(\omega) = \exp\left(-\frac{1}{2}\left(\frac{\sigma_z}{c}\omega\right)^2\right), \quad (2)$$

$$h(\omega) = \exp\left(-\left(\frac{\sigma_z}{c}\omega\right)^2\right),$$

are shown in Fig. 2 for positive frequencies. The RMS width of the functions \tilde{g} and h are $c/\sigma_z = 2\pi \cdot 636.1$ MHz and $c/(\sqrt{2}\sigma_z) = 2\pi \cdot 449.8$ MHz respectively.

1.2 The ATLAS vacuum chamber

The ATLAS collaboration operates general-purpose pp detector at the LHC. A vacuum chamber is installed which is accommodated to the needs of the installed

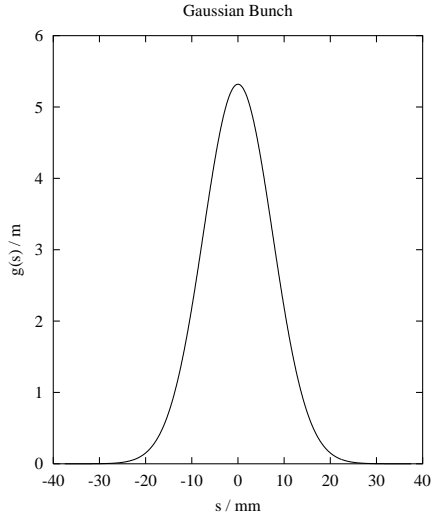


Figure 1: Gaussian bunch with an rms bunch length of $\sigma_z = 7.5$ cm. The function g is plotted versus the longitudinal position s in the bunch.

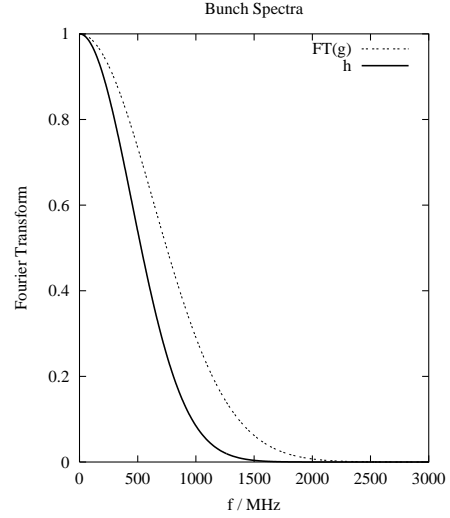


Figure 2: Fourier Transforms of the Gaussian bunch. The function \tilde{g} and h are plotted versus the frequency $\omega/(2\pi)$.

detector components. A 3D-view of the vacuum system is shown in Fig. 3.

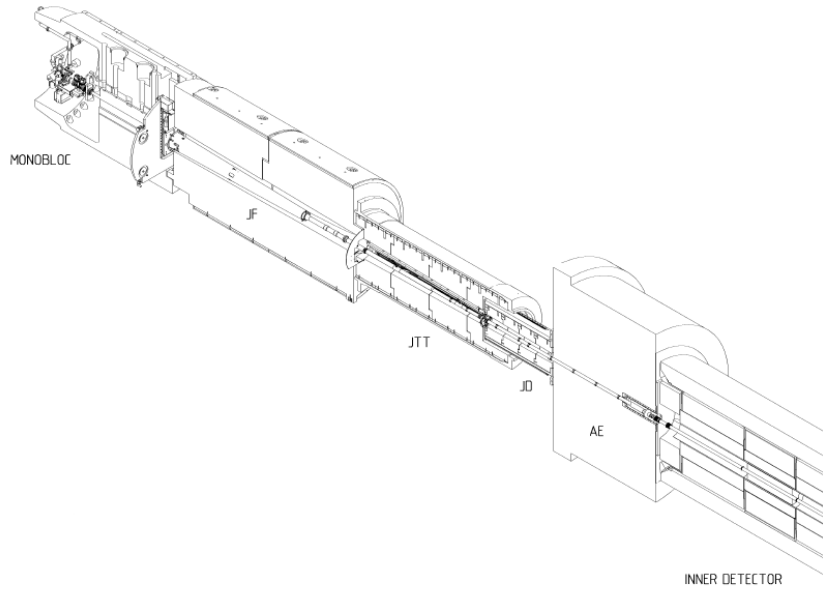


Figure 3: A 3D view of the ATLAS vacuum chamber [3]. The beam pipe is shown from monobloc module to the the interaction point in the inner detector.

The geometry of the ATLAS chamber is a cylindrically symmetric structure. A list of the r - z coordinates of the chamber is given in Table 2. A plot of the of r - z coordinates is shown in Fig. 4.

Name		Comments	z/mm	r/mm
ID	1	Inner Detector	0	23.5
	2		3650	23.5
AE	3	Pumping Port Start Pumping Port End Bellow Start Bellow End Bellow Start Bellow End	3690	23.5
	4		3710	29.0
	5		3786	29.0
	6		3846	29.0
	7		3934	29.0
	8		4088	29.0
	9		4334	29.0
	10		4488	29.0
	11		4540	29.0
JO	12	Bellow Start	4564	29.0
	13	Bellow End	4708	29.0
	14		9000	29.0
JTT	15		10446	29.0
	16		10487	41.5
	17		13207	41.5
JF	18	Bellow Start	13439	41.5
	19	Bellow End	13543	41.5
	20	Bellow Start	13747	41.5
	21	Bellow End	13851	41.5
	22		14311	41.5
	23		14411	60.0
	24		18499	60.0
MB	25	Monobloc	18639	23.0
	26		18716	23.0
	27		18734	20.0
	28		18964	20.0
	29		18984	17.0
	30		18999	17.0

Table 2: The main components of the ATLAS vacuum chamber.

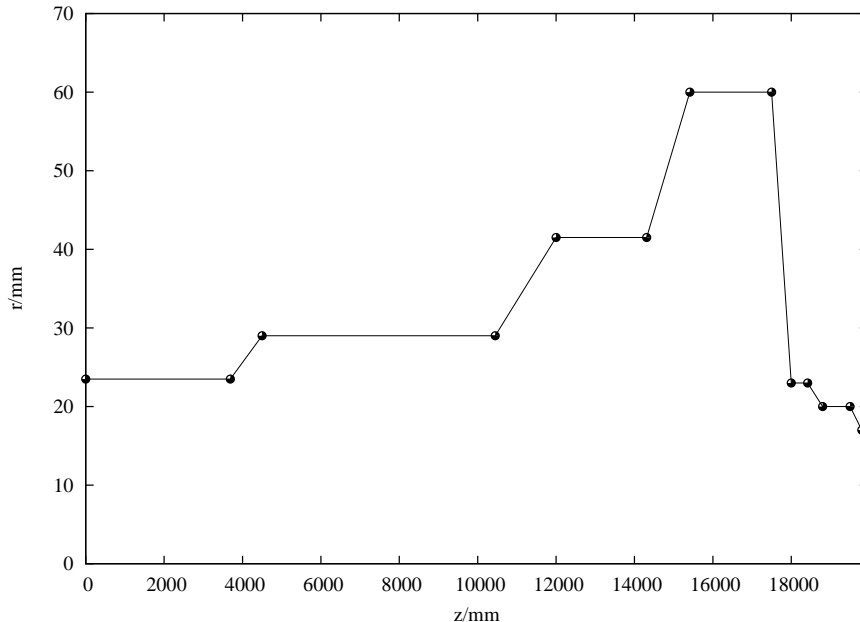


Figure 4: Schematic representation of the MAFIA model of the ATLAS vacuum chamber. All dimensions are in mm. The interaction point (IP) is at $z = 0$ mm

1.3 Wakefields and Higher Order Modes

A beam circulating in a storage ring interacts with its vacuum chamber surroundings via electromagnetic fields. These wake fields [4] in turn act back on the beam and can lead to instabilities, or may heat the vacuum chamber which can be a problem by itself or may cause a degeneration of the vacuum conditions in the beam pipe. The wake potential [4] of a bunch with a charge q_1 is defined as:

$$\mathbf{W}(\mathbf{r}_{\perp 2}, \mathbf{r}_{\perp 1}, s) = \frac{1}{q_1} \int_0^L dz (\mathbf{E} + c \mathbf{e}_z \times \mathbf{B})_{t=(z+s)/c}, \quad (3)$$

assuming that the bunch is ultra relativistic ($v = c$ or $\beta = 1$), which is a very good approximation for the LHC beam. The wake potential may be regarded as an average of the Lorentz force on a test charge q_2 . $\mathbf{r}_{\perp 1}$ and $\mathbf{r}_{\perp 2}$ are the transverse coordinates of the bunch with charge q_1 and the test charge q_2 .

If the structure traversed by the bunch is cylindrically symmetric then a multipole expansion can be used to describe the wake potential. The longitudinal wake potential is given by:

$$W_{\parallel}(r_1, r_2, \varphi_1, \varphi_2, s) = \sum_{m=0}^{\infty} r_1^m r_2^m W_{\parallel}^{(m)}(s) \cos(m(\varphi_2 - \varphi_1)). \quad (4)$$

The functions $W_{\parallel}^{(m)}(s)$ are the longitudinal m -pole wake potentials. It is often sufficient to consider only the leading terms of the series in equation (4), neglecting contributions from quadrupole and higher multipole components.

The longitudinal and transverse components of the wake potential are connected by the Panofsky–Wenzel theorem [5]. Integration of the transverse gradient (applied to the transverse coordinates of the test charge) of the longitudinal wake potential yields the transverse wake potential:

$$W_{\perp}^{(m)}(s) = - \int_{-\infty}^s d\zeta W_{\parallel}^{(m)}(\zeta), \quad (5)$$

for $m > 0$. There is no transverse monopole wake potential. The dipole wake potential does not depend on the position of the test charge q_2 . The kick on the test charge is linear in the offset of the point charge q_1 .

In Cartesian coordinates the longitudinal wake potential is approximately:

$$\begin{aligned} W_{\parallel}(x_1, y_1, x_2, y_2, s) &\approx W_{\parallel}^{(0)}(s) \\ &+ (x_2 x_1 + y_2 y_1) W_{\parallel}^{(1)}(s), \end{aligned} \quad (6)$$

while the transverse wake potential can be calculated using the Panofsky–Wenzel theorem:

$$\mathbf{W}_{\perp}(x_1, y_1, x_2, y_2, s) \approx (x_1 \mathbf{u}_x + y_1 \mathbf{u}_y) W_{\perp}^{(1)}(s), \quad (7)$$

with

$$W_{\perp}^{(1)}(s) = - \int_{-\infty}^s ds' W_{\parallel}^{(0)}(s'), \quad (8)$$

1.3.1 Loss and Kick Parameters

The numerical calculations provide the monopole and dipole wake potentials $W_{\parallel}^{(0)}(s)$ and $W_{\perp}^{(1)}(s)$. From the wake potentials the loss and kick parameters are obtained which are closely related to the impedance.

The total loss parameter is

$$k_{\parallel\text{tot}}^{(0)} = \int ds W_{\parallel}^{(0)}(s) g(s), \quad (9)$$

where $g(s)$ is the normalized charge density of the bunch, see Eqn.(1). The total loss parameter $k_{\parallel\text{tot}}^{(0)}$ characterizes the resistive part of the impedance and is closely related to the transient power loss P of the beam:

$$P = N_b f_R q_b^2 k_{\parallel\text{tot}}^{(0)}, \quad (10)$$

where N_b is the total number of bunches and q_b the single bunch charge, and f_R the revolution frequency (see Table 1).

The total (dipole) kick parameter is

$$k_{\perp}^{(1)} = \int ds W_{\perp}^{(1)}(s) g(s) \quad (11)$$

which is closely related to the transverse impedance (see [6])

$$(Z_{\perp})_{\text{eff}} = 2 \sqrt{\pi} \frac{\sigma_z}{c} k_{\perp}^{(1)}. \quad (12)$$

1.3.2 Higher Order Modes

Numerical calculations of the wake potentials in the time domain are complemented with a frequency domain analysis of the eigenmodes of the vacuum chamber. The eigenvalue solver provides the frequency ($f = \omega/(2\pi)$) and the electric and magnetic fields (\mathbf{E} , \mathbf{B}) for each mode on the mesh. In a first postprocessing step the stored energy U in the \mathbf{E} , and \mathbf{B} field of each mode, and the voltage $V(r) = \int dz E_z(r, z) \exp(i\omega z/c)$ is calculated. In a second step one obtains the loss parameter of the mode at radius r and the corresponding R/Q :

$$k_{\parallel}(r) = \frac{|V(r)|^2}{4U}, \quad (13)$$

$$\frac{R}{Q} = \frac{2k_{\parallel}(r)}{\omega}. \quad (14)$$

The loss parameter is measured in V/C and the R/Q in Ohm. Furthermore the Q -value is calculated

$$Q = \frac{\omega U}{P_{sur}} \quad (15)$$

from the field distribution on the wall of the vacuum chamber and surface resistivity. P_{sur} is the power dissipated into the cavity wall due to the surface resistivity R_{sur} . In the post-processor the dissipated power P_{sur} is often calculated for a copper surface with resistivity:

$$R_{Cu} = \sqrt{\frac{\omega \mu_0}{2 \sigma_{Cu}}}, \quad \sigma_{Cu} = 5.8 \cdot 10^7 (\Omega \text{ m})^{-1}. \quad (16)$$

The Q -value of any material can be found by scaling the value for copper:

$$Q_{Mat} = \sqrt{\frac{\sigma_{Mat}}{\sigma_{Cu}}} Q_{Cu}, \quad (17)$$

where σ_{Mat} is the conductivity of the material. For steel the conductivity is approximately [7] $\sigma_{St} = 1.5 \cdot 10^6 (\Omega \text{ m})^{-1}$. A purely geometric property of the chamber is the parameter G_1 [8], which is defined as:

$$G_1 = R_{Cu} Q_{Cu}. \quad (18)$$

For monopole modes the loss parameter $k_{\parallel}(r)$ is calculated on axis ($r = 0$) and the corresponding R/Q is denoted as:

$$\frac{R^{(0)}}{Q} = \frac{2 k_{\parallel}(r = 0)}{\omega}. \quad (19)$$

The beam interacts with dipole modes only in the case that the beam traverses the vacuum chamber off axis since the longitudinal electric field of any dipole mode vanishes on axis. The loss parameters of dipole modes are calculated for an offset of $r = 1$ cm from the axis of the vacuum chamber. From the loss parameters the $R^{(1)}/Q$ parameter and the transverse impedance is obtained using the following relations:

$$\frac{R^{(1)}}{Q} = \frac{1}{r^2} \frac{2 k_{\parallel}(r)}{\omega}, \quad (20)$$

$$Z_{\perp} = \frac{1}{\omega/c} \frac{R^{(1)}}{Q} Q_{Steel}. \quad (21)$$

The units of $R^{(1)}/Q$ and for Z_{\perp} are Ohm/m² and Ohm/m respectively.

The long range wake potential of HOMs for a point charge are ¹:

$$\mathcal{W}_{\parallel}^{(m)}(s) = - \sum_n \omega_n \left(\frac{R^{(m)}}{Q} \right)_n \cos(\omega_n s/c) \exp(-1/\tau_n s/c) \quad (22)$$

$$\mathcal{W}_{\perp}^{(1)}(s) = c \sum_n \left(\frac{R^{(1)}}{Q} \right)_n \sin(\omega_n s/c) \exp(-1/\tau_n s/c),$$

where $m = 0$ is the longitudinal monopole and $m = 1$ the longitudinal dipole wake potential, and τ_n is the damping time for mode n :

$$\tau_n = \frac{2 Q_n}{\omega_n}. \quad (23)$$

The long range wake potential of a Gaussian bunch is the convolution of the wake potentials $\mathcal{W}_{\parallel}^{(m)}(s)$ or $\mathcal{W}_{\perp}^{(1)}(s)$ with a the charge distribution $g(s)$ (Fig. 1):

$$\mathcal{W}_{\parallel}^{(m)}(s) = \int_{-\infty}^{\infty} d\bar{s} g(s - \bar{s}) \mathcal{W}_{\parallel}^{(m)}(\bar{s}) \quad (24)$$

$$\mathcal{W}_{\perp}^{(1)}(s) = \int_{-\infty}^{\infty} d\bar{s} g(s - \bar{s}) \mathcal{W}_{\perp}^{(1)}(\bar{s}).$$

¹It has been assumed that the Q-values of the HOMs are large and the sin-like contribution to the longitudinal wake has been neglected.

2 Wakefields

Since the ATLAS vacuum chamber is rotationally symmetric with respect to the longitudinal axis it is convenient to use a two dimensional (r, z) computer code for numerical wakefield calculations. The ECHO2D [9, 10] code was used to calculate the Monopole and Dipole wakefield of the ATLAS vacuum chamber. Firstly the geometry, which is shown in Fig. 5, was used. In this geometry the bellows of the ATLAS chamber, which are listed in Table 2, are not included. In a second step the wakefields of one of the bellows were calculated and in a third step the ATLAS vacuum chamber and two bellows were investigated.

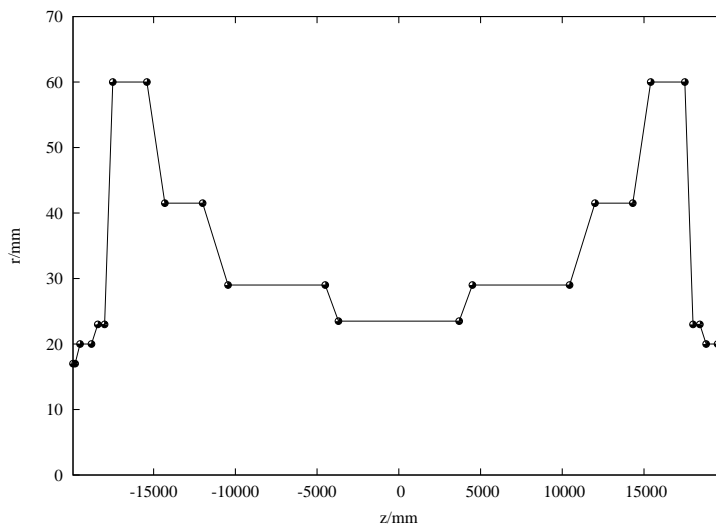


Figure 5: Schematic representation of the ECHO2D model of the ATLAS vacuum chamber. All dimensions are in mm. The interaction point (IP) is at $z = 0$ mm.

2.1 Wakefields of the ATLAS chamber without bellows

The longitudinal monopole, the longitudinal dipole, and the transverse dipole wake potentials, which are calculated with the ECHO2D code, are shown in Fig. 6, Fig. 7, and Fig. 8. The results for the loss and kick parameters are summarized in Table 3. The longitudinal short range wakes correspond to an almost purely inductive impedance. The loss parameter is very small.

Parameter	Results	$\Delta z/\text{cm}$	$\Delta r/\text{cm}$
$k_{\parallel\text{tot}}^{(0)}$ (V/nC)	$1.08 \cdot 10^{-6}$	0.2	0.1
$k_{\perp}^{(1)}$ (V/pCm)	1.72	0.2	0.1

Table 3: Results for the loss and kick parameters of the ATLAS vacuum chamber for a Gaussian bunch with rms bunch length of $\sigma_z = 7.5$ cm.

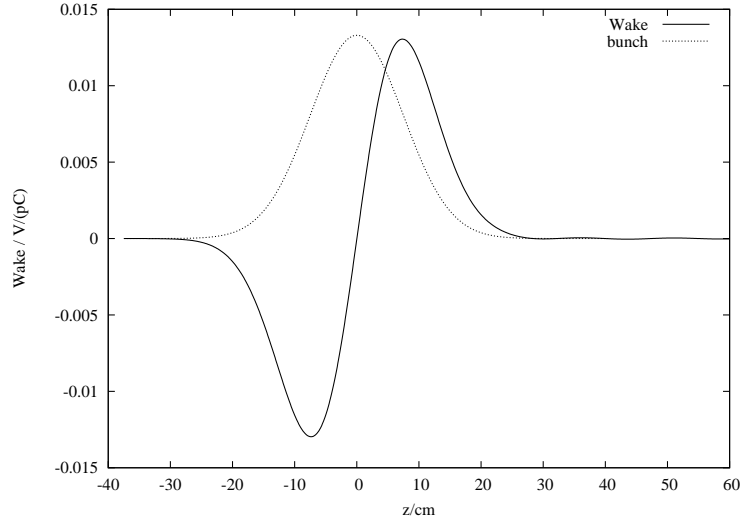


Figure 6: Longitudinal monopole wake potential of the ATLAS vacuum chamber. The wake has been calculated with the ECHO2D code for an rms bunch length of 7.5 cm. For the calculation a step size of $\Delta z = 2$ mm in the longitudinal and of $\Delta r = 1$ mm in the radial have been used. The bunch shape is also shown (in arbitrary units).

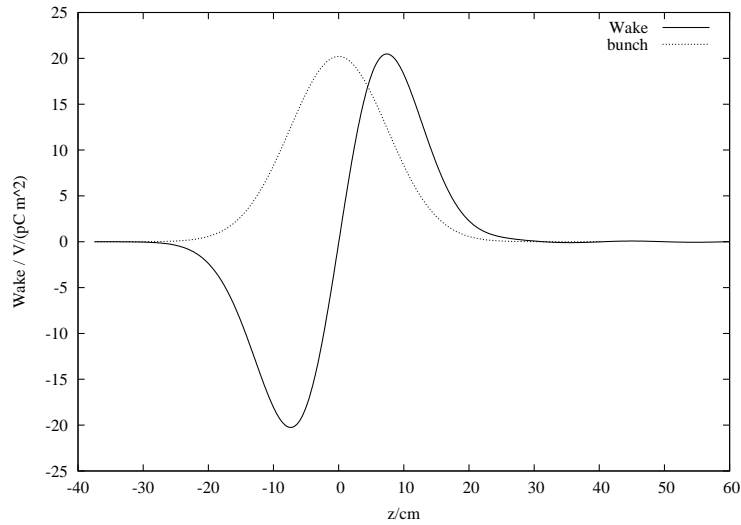


Figure 7: Longitudinal dipole wake potential of the ATLAS vacuum chamber. The wake has been calculated with the ECHO2D code for an rms bunch length of 7.5 cm. For the calculation a step size of $\Delta z = 2$ mm in the longitudinal and of $\Delta r = 1$ mm in the radial have been used. The bunch shape is also shown (in arbitrary units).

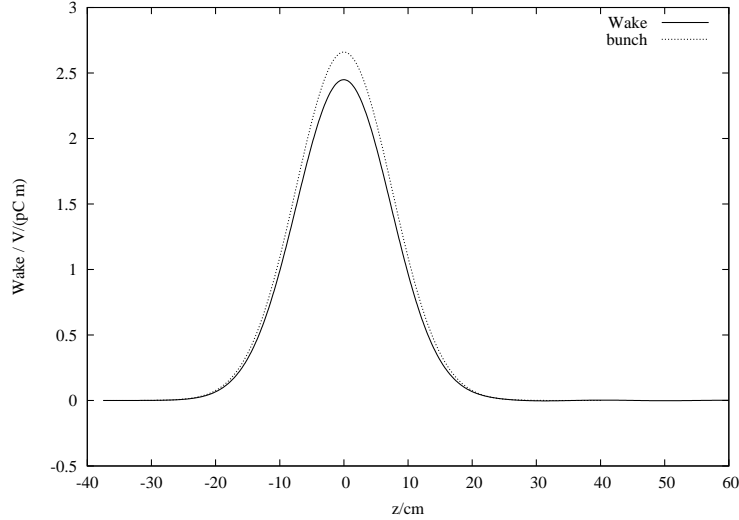


Figure 8: Transverse dipole wake potential of the ATLAS vacuum chamber. The wake has been calculated with the ECHO2D code for an rms bunch length of 7.5 cm. For the calculation a step size of $\Delta z = 2$ mm in the longitudinal and of $\Delta r = 1$ mm in the radial have been used. The bunch shape is also shown (in arbitrary units).

The longitudinal monopole ($m = 0$) and dipole ($m = 1$) impedance can be approximated for small frequencies ω as:

$$Z_{\parallel}^{(m)}(\omega) \approx -i\omega L^{(m)}, \quad (25)$$

with an inductance $L^{(m)}$. The corresponding wake potential for a Gaussian bunch is [11]

$$W_{\parallel}^{(m)}(s) = -L^{(m)} c^2 \frac{d}{ds} g(s), \quad (26)$$

where $g(s)$ is the Gaussian charge distribution (Eqn.(1)). The transverse dipole impedance is obtained from the longitudinal dipole impedance:

$$Z_{\perp}^{(1)}(\omega) = \frac{c}{\omega} Z_{\parallel}^{(1)}(\omega) = -i c L^{(1)}. \quad (27)$$

The corresponding transverse dipole wake potential for a Gaussian bunch is [12]:

$$W_{\perp}^{(1)}(s) = c^2 L^{(1)} g(s). \quad (28)$$

The total loss parameter of this wake potential is simply

$$k_{\perp}^{(1)} = c^2 L^{(1)} \int ds g(s)^2 = \frac{c^2}{2\sigma_z \sqrt{\pi}} L^{(1)}. \quad (29)$$

The inductance $L^{(1)}$ can be calculated from the kick parameter if the wake is proportional to the charge distribution (Eqn. (28)) which is a very good approximation for the transverse wake of the ATLAS chamber, see Fig. 8. One obtains $5.1 \mu\text{H}/\text{m}^2$ for the inductance $L^{(1)}$ using the kick parameter from Table 5. This corresponds to an impedance of $Z_{\parallel}^{(1)}$ of $-i c L^{(1)} = -i 1.52 \text{ k}\Omega/\text{m}$.

2.2 Wakefields of one bellow

There are several unshielded bellows installed around the interaction region of the ATLAS experiment. The positions of the vacuum chamber sections with bellows are listed in Table 2. All bellows have similar dimensions. The wakefields of the bellow in the AE section were investigated in detail. A technical drawing of the bellow with the geometrical dimension is shown in Fig. 9.

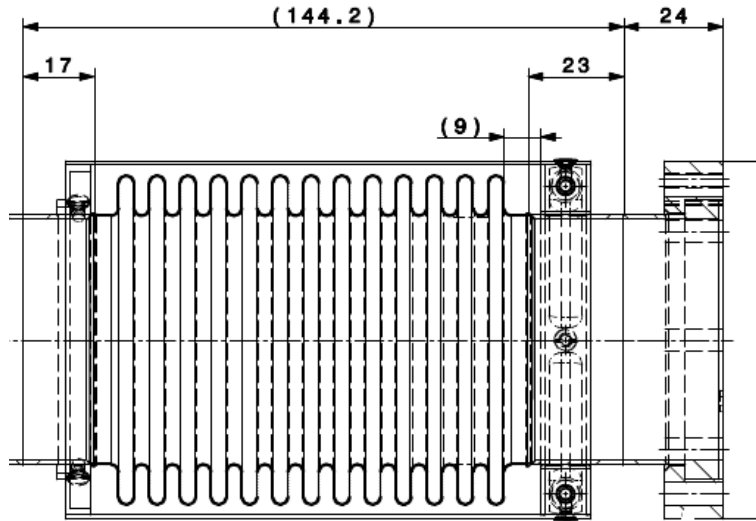


Figure 9: One of the bellows in the ATLAS vacuum chamber [13]. The technical drawing shows the dimensions of the bellow of the AE section in mm.

The longitudinal (monopole) and the transverse dipole wake potentials, which are calculated with the ECHO2D code, are shown in Fig. 10, and Fig. 11 for a mesh step size of $\Delta z = 1 \text{ mm}$ and $\Delta r = 0.5 \text{ mm}$. The results for the loss and kick parameters for one bellow in the section AE of the ATLAS vacuum chamber are summarized in Table 4 for two different step sizes of the mesh. The loss parameter is zero within the numerical accuracy of the ECHO2D code, but the kick parameter of *one* bellow is slightly larger than the kick parameter of the ATLAS chamber without bellows (Fig. 5). The transverse short range wakefield is therefore clearly dominated by the wakefields of the unshielded bellows.

The mesh size has only a small impact on the results. The transverse wake potential for different mesh sizes is shown in Fig. 12.

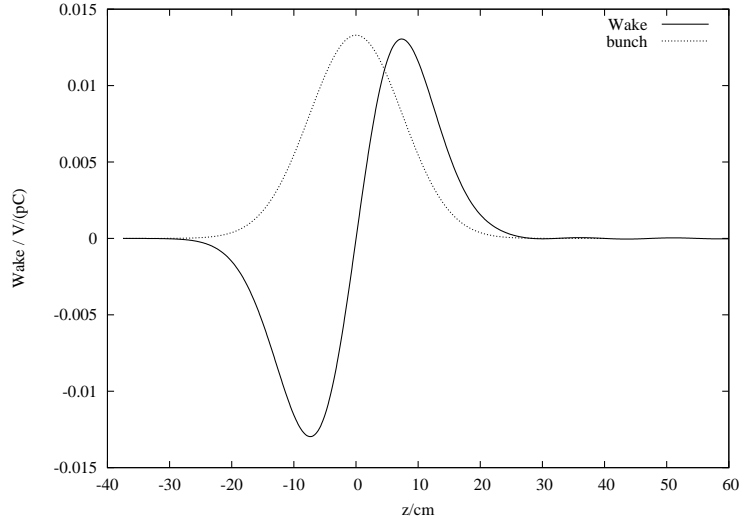


Figure 10: Longitudinal monopole wake potential of the bellow in the section AE of the ATLAS vacuum chamber. The wake has been calculated with the ECHO2D code for an rms bunch length of 7.5 cm. For the calculation a step size of $\Delta z = 1$ mm in the longitudinal and of $\Delta r = 0.5$ mm in the radial have been used. The bunch shape is also shown (in arbitrary units).

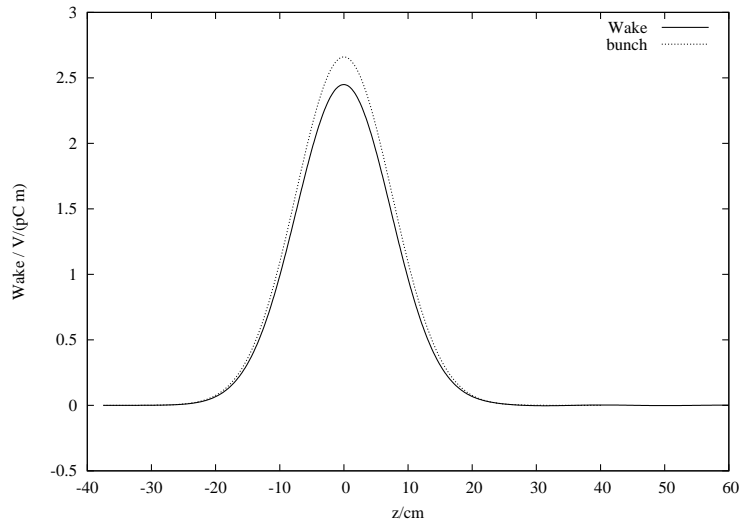


Figure 11: Transverse dipole wake potential of the bellow in the section AE of the ATLAS vacuum chamber. The wake has been calculated with the ECHO2D code for an rms bunch length of 7.5 cm. For the calculation a step size of $\Delta z = 1$ mm in the longitudinal and of $\Delta r = 0.5$ mm in the radial have been used. The bunch shape is also shown (in arbitrary units).

Parameter	$\Delta z = 0.1 \text{ cm}$	$\Delta z = 0.2 \text{ cm}$
	$\Delta r = 0.05 \text{ cm}$	$\Delta r = 0.1 \text{ cm}$
$k_{\parallel \text{tot}}^{(0)}$ (V/nC)	0.0000	0.0000
$k_{\perp}^{(1)}$ (V/pCm)	1.9998	1.9142

Table 4: Results for the loss and kick parameters calculated for the one bellow for a Gaussian bunch with rms bunch length of $\sigma_z = 7.5 \text{ cm}$ and two different step sizes of the mesh.

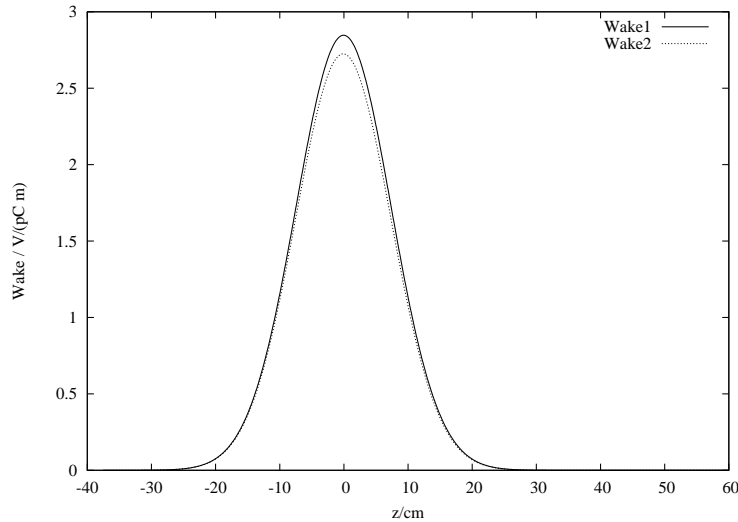


Figure 12: Comparison of transverse dipole wake potentials of one bellow in the section AE of the ATLAS vacuum chamber which have been calculated with different mesh size. For the calculation of the Wake1 a step size of $\Delta z = 1 \text{ mm}$ in the longitudinal and of $\Delta r = 0.5 \text{ mm}$ in the radial have been used. For the calculation of the Wake2 a step size of $\Delta z = 2 \text{ mm}$ and of $\Delta r = 1 \text{ mm}$ have been used.

2.3 Wakefields of the ATLAS chamber with bellows

In the previous section the wakefields of one bellow have been calculated assuming that the bellow is connected at both sides with a smooth round vacuum pipe. Now two bellows are placed at symmetric positions around the IP within the ATLAS vacuum chamber (Fig. 5). The results for the transverse dipole wake potential are shown in Fig. 13. The kick parameter $k_{\perp}^{(1)}$ for this structure is equal to 4.11 V/pCm which is smaller than the sum of the kick parameters from the ATLAS chamber (Table 3) and the kick parameter of two bellows (Table 4) of 5.54 V/pCm . The results of the wakefield calculations are summarized in the following Table 5 in terms of kick parameters and the corresponding dipole

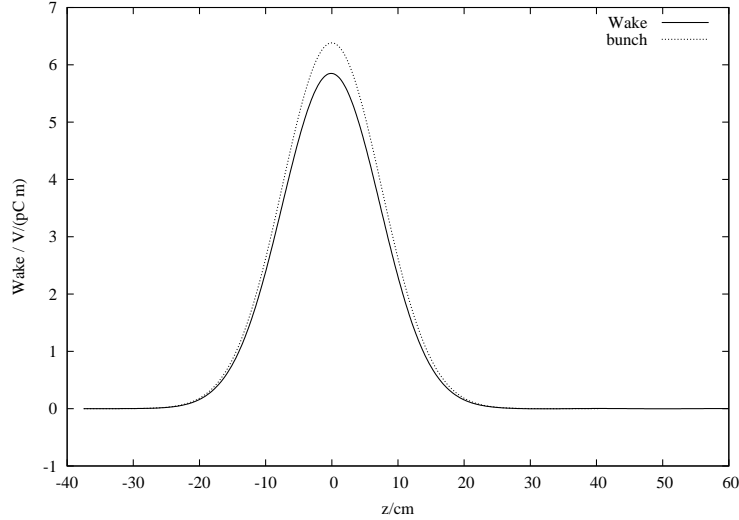


Figure 13: Transverse dipole wake potential of the ATLAS vacuum chamber and 2 bellows installed in the sections AE. The wake has been calculated with the ECHO2D code for an rms bunch length of 7.5 cm. For the calculation a step size of $\Delta z = 2$ mm in the longitudinal and of $\Delta r = 1$ mm in the radial have been used. The bunch shape is also shown (in arbitrary units).

impedance, which is based on the approximation with an inductance $L^{(1)}$, see Eqn. (28).

Vacuum chamber	Kick parameter $k_{\perp}^{(1)}$ (V/pCm)	Impedance $Z_{\perp}^{(1)}(\omega)$ (k Ω /m)
ATLAS w/o bellows	1.72	$-i 1.52$
one bellow	1.99	$-i 1.76$
ATLAS w. two bellows	4.11	$-i 3.64$
Sum ATLAS + 10 bellows	21.6	$-i 19.2$

Table 5: Results for kick parameters and the transverse impedance calculated for a Gaussian bunch with rms bunch length of $\sigma_z = 7.5$ cm and using a mesh with step sizes of $\Delta z = 0.2$ cm and $\Delta r = 0.1$ cm.

3 Higher Order Modes - HOMs

The electric and magnetic fields of the higher order modes are calculated with the frequency domain solver of the computer code MAFIA [14, 15, 16]. A 2-dimensional model of the ATLAS vacuum chamber (see Fig.4) has been used since it is sufficient to model a cylindrically symmetric structure on a $r - z$ -grid to obtain all important rf-parameters. The step size of the mesh was 1 mm in the radial (r) and 2 mm in the longitudinal (z) direction. Different sets of boundary conditions (electric or E and magnetic or M) were used at both ends of the modeled structure. The MAFIA [15] eigenvalue solver was used to calculate monopole and dipole modes. The results of calculations turned out to be independent from the boundary conditions and they are presented for electric (E) boundary conditions on both ends in the tables 6 and 7 for monopole modes and in the tables 8 and 9 for dipole modes. The modes are labeled as "EE-n" according to the boundary conditions and the mode number n, starting with the label "EE-1" for the mode with the lowest frequency. The loss parameters, R/Q and Q-values are obtained during a post processing step according to section 1.3.2 of this report.

3.1 Monopole Modes

Most of the higher order monopole modes are trapped in the region between 14.5 m to 18.5 m from the IP. The mode with largest loss parameter is the mode EE-31. The electric field of mode EE-31 ($f = 2206.0$ MHz, $k^{(0)} = 0.3941$ V/nC) is shown in Fig. 14. Modes with a frequency of about and above 2.8 GHz are not completely trapped in the region 14.5 m to 18.5 m from the IP but leak out into the neighboring regions with a smaller radius. The electric field of mode EE-59 ($f = 2798.4$ MHz, $k^{(0)} = 0.0011$ V/nC) is plotted in Fig. 15 in the two regions between 14 m to 15 m and 18 m to 19 m from the IP.

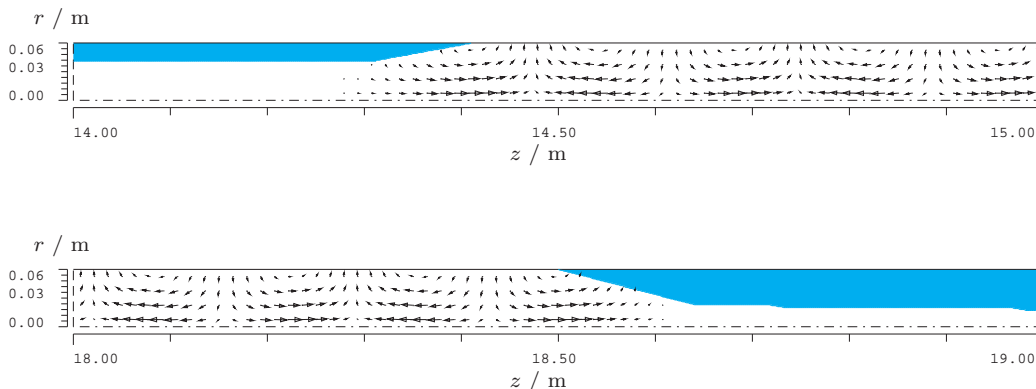


Figure 14: The electric field of monopole mode EE-31 in the ATLAS vacuum chamber.

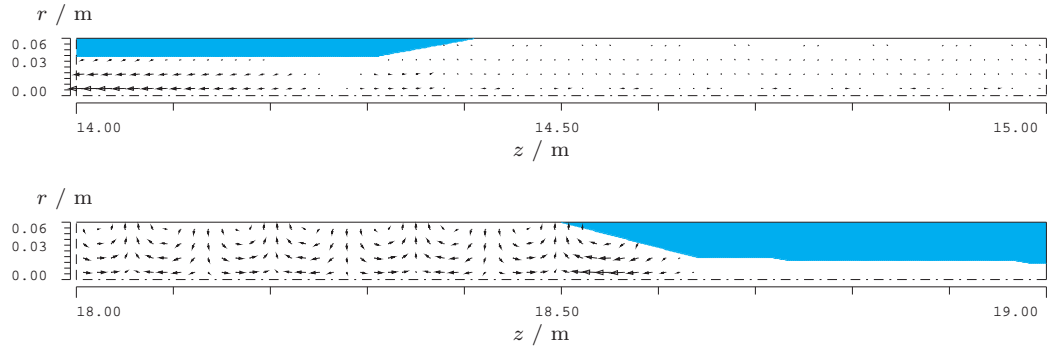
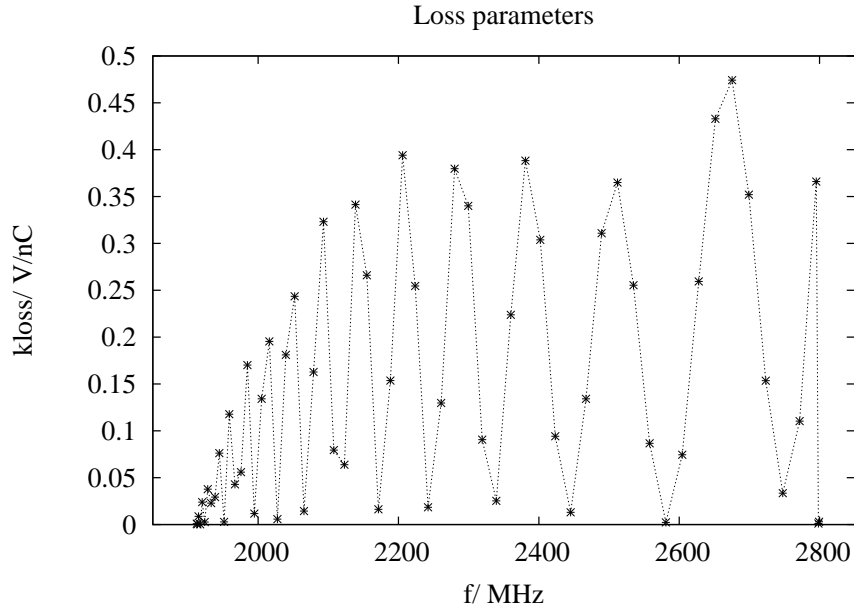


Figure 15: The electric field of monopole mode EE-59 in the ATLAS vacuum chamber.

The loss parameters of the monopole modes from Tables 6 and 7 are plotted versus the mode frequency in Fig. 16.



Mode	f/MHz	$k^{(0)}$ (V/nC)	G_1 (Ohm)	R/Q (Ohm)	Q_{Cu}	Q_{Steel}
EE-1	1912.6	0.0009	445.7	0.0002	39061	6281
EE-2	1913.5	0.0002	445.9	0.0000	39070	6283
EE-3	1915.2	0.0087	446.2	0.0014	39084	6285
EE-4	1917.5	0.0002	446.7	0.0000	39104	6288
EE-5	1920.4	0.0240	447.4	0.0040	39130	6292
EE-6	1924.1	0.0028	448.1	0.0005	39161	6297
EE-7	1928.2	0.0378	449.1	0.0062	39199	6303
EE-8	1933.1	0.0228	450.1	0.0038	39241	6310
EE-9	1938.6	0.0293	451.3	0.0048	39290	6318
EE-10	1944.8	0.0762	452.7	0.0125	39344	6327
EE-11	1951.6	0.0028	454.1	0.0004	39404	6336
EE-12	1959.0	0.1177	455.8	0.0191	39469	6347
EE-13	1967.0	0.0428	457.5	0.0069	39540	6358
EE-14	1975.6	0.0559	459.4	0.0090	39617	6371
EE-15	1984.8	0.1701	461.4	0.0273	39699	6384
EE-16	1994.6	0.0117	463.6	0.0019	39786	6398
EE-17	2005.0	0.1342	465.9	0.0213	39879	6413
EE-18	2016.0	0.1954	468.3	0.0309	39977	6428
EE-19	2027.4	0.0058	470.8	0.0009	40080	6445
EE-20	2039.5	0.1811	473.5	0.0283	40188	6462
EE-21	2052.1	0.2435	476.3	0.0378	40301	6481
EE-22	2065.3	0.0144	479.2	0.0022	40419	6500
EE-23	2079.0	0.1628	482.3	0.0249	40542	6519
EE-24	2093.2	0.3231	485.4	0.0491	40669	6540
EE-25	2107.9	0.0794	488.7	0.0120	40801	6561
EE-26	2123.1	0.0639	492.1	0.0096	40937	6583
EE-27	2138.7	0.3414	495.6	0.0508	41077	6605
EE-28	2154.9	0.2659	499.2	0.0393	41221	6629
EE-29	2171.4	0.0163	502.9	0.0024	41369	6652
EE-30	2188.5	0.1536	506.8	0.0223	41520	6677

Table 6: Monopole modes of the ATLAS vacuum chamber.

Mode	f/MHz	$k^{(0)}$ (V/nC)	G_1 (Ohm)	R/Q (Ohm)	Q_{Cu}	Q_{Steel}
EE-31	2206.0	0.3941	510.7	0.0569	41675	6702
EE-32	2223.9	0.2546	514.7	0.0364	41833	6727
EE-33	2242.2	0.0184	518.8	0.0026	41994	6753
EE-34	2260.9	0.1297	523.0	0.0183	42158	6779
EE-35	2280.0	0.3796	527.3	0.0530	42325	6806
EE-36	2299.4	0.3401	531.6	0.0471	42494	6833
EE-37	2319.3	0.0905	536.0	0.0124	42664	6861
EE-38	2339.5	0.0253	540.6	0.0034	42837	6888
EE-39	2360.0	0.2238	545.1	0.0302	43011	6916
EE-40	2380.8	0.3883	549.8	0.0519	43186	6945
EE-41	2402.0	0.3038	554.4	0.0403	43361	6973
EE-42	2423.5	0.0943	559.2	0.0124	43537	7001
EE-43	2445.2	0.0130	563.9	0.0017	43712	7029
EE-44	2467.2	0.1341	568.7	0.0730	43887	7057
EE-45	2489.5	0.3108	573.5	0.0397	44060	7085
EE-46	2512.0	0.3650	578.4	0.0462	44231	7113
EE-47	2534.8	0.2554	583.2	0.0321	44399	7140
EE-48	2557.8	0.0867	588.0	0.0108	44562	7166
EE-49	2581.0	0.0023	592.8	0.0003	44722	7192
EE-50	2604.3	0.0744	597.5	0.0091	44875	7216
EE-51	2627.8	0.2595	602.1	0.0314	45021	7240
EE-52	2651.5	0.4330	606.7	0.0520	45160	7262
EE-53	2675.4	0.4743	611.1	0.0564	45288	7283
EE-54	2699.3	0.3520	615.4	0.0415	45403	7301
EE-55	2723.3	0.1536	619.5	0.0179	45498	7316
EE-56	2747.5	0.0335	622.9	0.0039	45553	7325
EE-57	2771.6	0.1103	624.9	0.0127	45497	7316
EE-58	2795.2	0.3660	610.4	0.0417	44253	7116
EE-59	2798.4	0.0011	442.7	0.0001	32078	5158
EE-60	2799.2	0.0030	443.5	0.0003	32132	5167

Table 7: Monopole modes of the ATLAS vacuum chamber.

Summing up the contributions from monopole modes one obtains for the longitudinal impedance due to HOMs:

$$Z_{||}(\omega) = \sum_n \frac{R_n^{(0)}}{1 - i Q_n (\omega/\omega_n - \omega_n/\omega)}, \quad (30)$$

where

$$R_n^{(0)} = Q_{Steel} \left(\frac{R^{(0)}}{Q} \right)_n \quad (31)$$

is the shunt impedance of mode n . The real part of the longitudinal impedance is plotted in Fig. 17

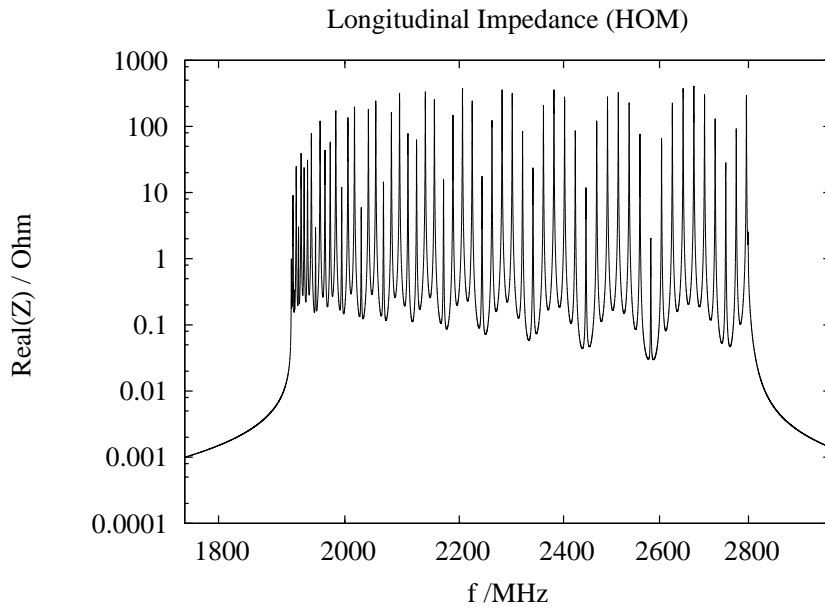


Figure 17: Real part of the longitudinal impedance due to HOMs using the data from Tables 6 and 7.

3.2 Dipole Modes

Also most of the higher order dipole modes are trapped in the region between 14.5 m to 18.5 m from the IP. One example is the the mode EE-22 ($f = 1660.1$ MHz, $k^{(1)}(r)/r^2 = 129.43$ V/(nC m²)) The electric field is shown in Fig. 18. But there are also modes with leak out into the neighboring regions with a smaller radius. The electric field of mode EE-45 ($f = 2143.0$ MHz, $k^{(1)}(r)/r^2 = 0.04$ V/(nC m²)) is plotted in Fig. 19 in the two regions between 14 m to 15 m and 18 m to 19 m from the IP. This is the mode with the lowest frequency which is not trapped region between 14.5 m to 18.5 m.

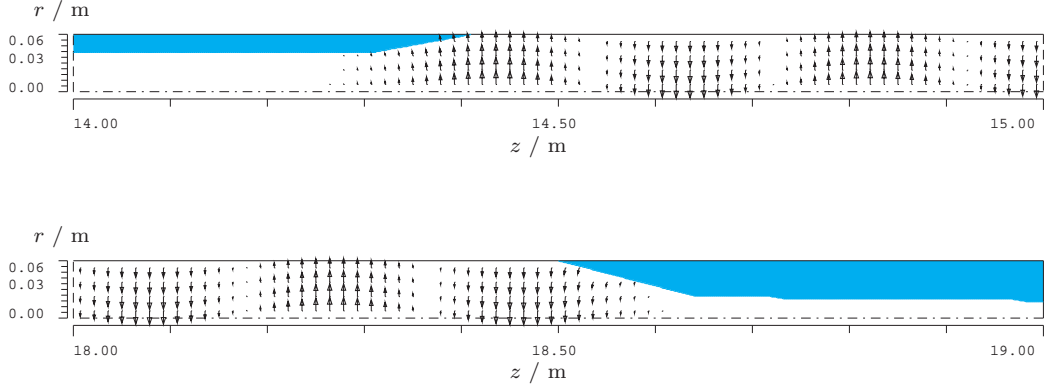


Figure 18: The electric field of dipole mode EE-22 in the ATLAS vacuum chamber.

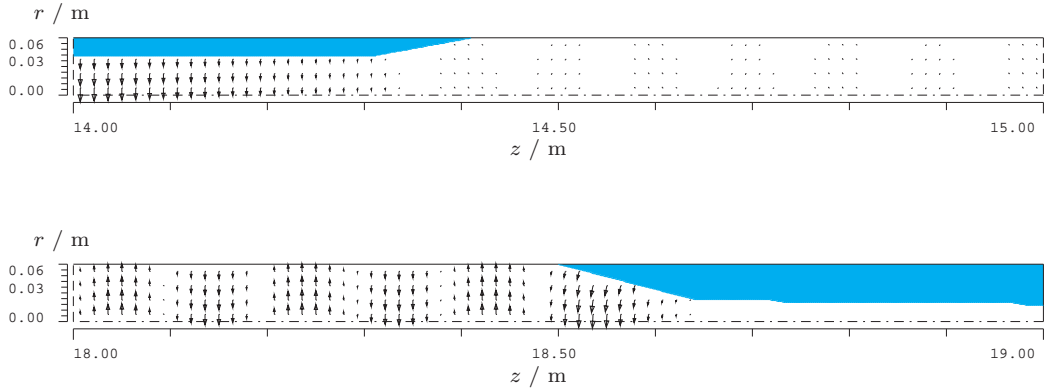


Figure 19: The electric field of dipole mode EE-45 in the ATLAS vacuum chamber.

Mode	f/MHz	$k^{(1)}(r)/r^2$ $/(V/(nCm^2))$	G_1 (Ohm)	Q_{Cu}	Q_{Steel}	Z_{\perp} /Ohm/m
EE-1	1464.6	0.17	244.7	24509	3941	4.80
EE-2	1465.9	0.40	245.2	24550	3948	11.15
EE-3	1468.1	1.91	246.1	24618	3958	53.38
EE-4	1471.1	0.71	247.3	24714	3974	19.81
EE-5	1475.0	6.79	248.9	24837	3994	189.27
EE-6	1479.7	0.03	250.8	24987	4018	0.91
EE-7	1485.3	13.33	253.0	25163	4046	371.46
EE-8	1491.7	4.28	255.6	25366	4079	119.15
EE-9	1498.9	10.78	258.5	25596	4116	300.04
EE-10	1506.9	24.19	261.8	25851	4157	672.68
EE-11	1515.7	0.09	265.4	26133	4202	2.45
EE-12	1525.3	34.31	269.4	26439	4251	952.08
EE-13	1535.7	27.79	273.7	26771	4305	770.41
EE-14	1546.8	2.65	278.3	27127	4362	73.49
EE-15	1558.6	57.50	283.3	27507	4423	1589.94
EE-16	1571.1	40.96	288.6	27910	4488	1130.94
EE-17	1584.4	1.54	294.3	28336	4556	42.43
EE-18	1598.2	70.49	300.2	28785	4629	1940.03
EE-19	1612.8	80.82	306.5	29255	4704	2219.85
EE-20	1628.0	5.56	313.1	29746	4783	152.32
EE-21	1643.7	43.89	320.0	30257	4865	1200.28
EE-22	1660.1	129.43	327.3	30787	4951	3531.26
EE-23	1677.1	76.29	334.8	31335	5039	2075.94
EE-24	1694.6	0.39	342.6	31901	5130	10.50
EE-25	1712.6	73.82	350.7	32483	5223	1996.45
EE-26	1731.1	172.18	359.1	33080	5319	4641.43
EE-27	1750.1	119.11	367.7	33691	5418	3199.79
EE-28	1769.6	10.61	376.6	34314	5518	284.04
EE-29	1789.6	38.26	385.7	34948	5620	1019.72
EE-30	1809.9	171.11	395.0	35592	5723	4539.97

Table 8: Dipole modes of the ATLAS vacuum chamber.

Mode	f/MHz	$k^{(1)}(r)/r^2$ $/(V/(nCm^2))$	G_1 (Ohm)	Q_{Cu}	Q_{Steel}	Z_{\perp} /Ohm/m
EE-31	1830.7	217.59	404.6	36243	5828	5746.53
EE-32	1851.9	116.28	414.3	36900	5934	3055.70
EE-33	1873.4	8.55	424.1	37560	6040	223.56
EE-34	1895.3	35.87	434.1	38222	6146	932.05
EE-35	1917.5	168.09	444.2	38882	6252	4341.09
EE-36	1940.0	259.10	454.3	39537	6358	6647.86
EE-37	1962.8	218.59	464.5	40184	6462	5568.34
EE-38	1985.9	94.18	474.6	40817	6564	2380.83
EE-39	2009.2	5.71	484.5	41428	6662	143.03
EE-40	2032.7	29.80	494.1	42005	6755	739.80
EE-41	2056.5	146.17	503.1	42526	6838	3589.39
EE-42	2080.4	269.45	511.0	42943	6905	6529.24
EE-43	2104.3	318.11	516.1	43125	6935	7566.55
EE-44	2128.1	263.82	510.5	42419	6821	6034.87
EE-45	2143.0	0.04	244.9	20275	3260	0.42
EE-46	2144.0	2.81	246.0	20360	3274	30.39
EE-47	2145.7	0.71	248.7	20582	3309	7.78
EE-48	2147.9	25.17	258.6	21385	3439	284.93
EE-49	2150.3	40.49	300.9	24871	3999	531.91
EE-50	2152.5	62.34	301.1	24878	4000	817.43
EE-51	2155.7	16.37	265.9	21951	3530	188.83
EE-52	2159.9	4.11	258.9	21355	3434	45.90
EE-53	2164.8	13.14	260.3	21443	3448	146.84
EE-54	2170.1	18.78	271.0	22299	3586	217.20
EE-55	2175.0	3.18	313.2	25740	4139	42.26
EE-56	2179.3	40.85	310.7	25514	4103	535.97
EE-57	2185.1	10.16	278.8	22864	3676	118.86
EE-58	2191.9	19.68	279.2	22854	3675	228.59
EE-59	2198.6	8.52	309.6	25306	4069	108.89
EE-60	2204.2	44.09	333.2	27200	4374	602.83

Table 9: Dipole modes of the ATLAS vacuum chamber.

The loss parameters of the dipole modes from Tables 8 and 9 at a radius $r = 1$ cm are plotted versus the mode frequency in Fig. 20.

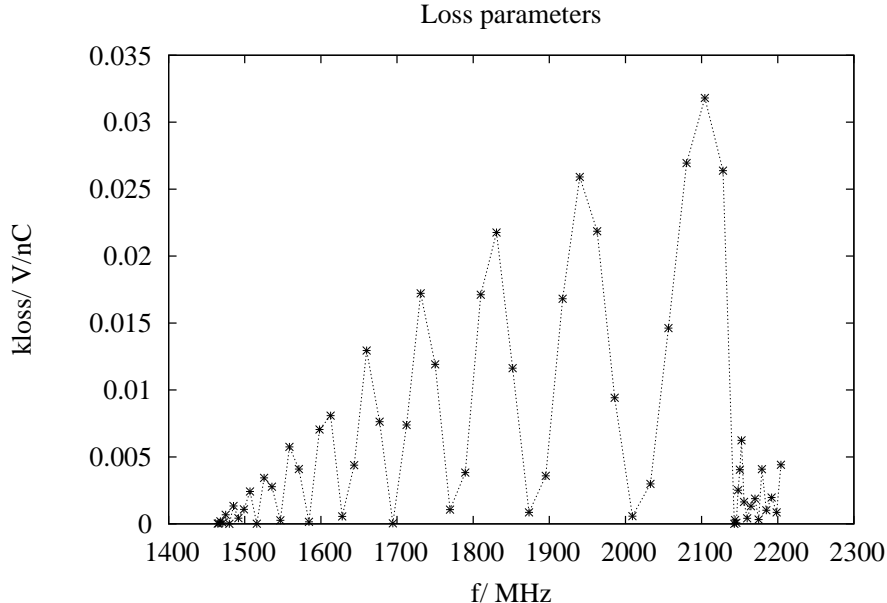


Figure 20: Plot of the loss parameters of the dipole modes at an offset of $r = 1$ cm versus frequency using the data from Tables 8 and 9. The data points are marked with stars. (The dotted line is intended only to guide the eye.)

The transverse (dipole) impedance due to HOMs can be obtained as a sum over all considered dipole modes:

$$Z_{\perp}(\omega) = \sum_n \frac{Z_{\perp n}}{Q_n} \frac{i\omega_n^2}{\omega^2 - \omega_n^2 + i\omega\omega_n/Q_n}, \quad (32)$$

where $Z_{\perp n}$ is the transverse impedance of the mode n (unit Ohm/m) which is listed in the rightmost column of the Tables 8 and 9.

The real part of the transverse impedance is plotted in Fig. 21

4 Summary

The wakefields and higher order modes of the new beam pipe of the ATLAS detector for the High Luminosity LHC configuration (HL-LHC) have been calculated with the ECHO2D [9, 10] and MAFIA [14] using a 2D model of the vacuum chamber. The radius of the central beam pipe is 23.5 mm while the radius in the JF section (about 14.5 m to 18.5 m from the IP) is 60.0 mm. In that region several HOMs are trapped, but the loss parameters are quite small ($k_{\parallel} \leq 0.5$ V/nC).

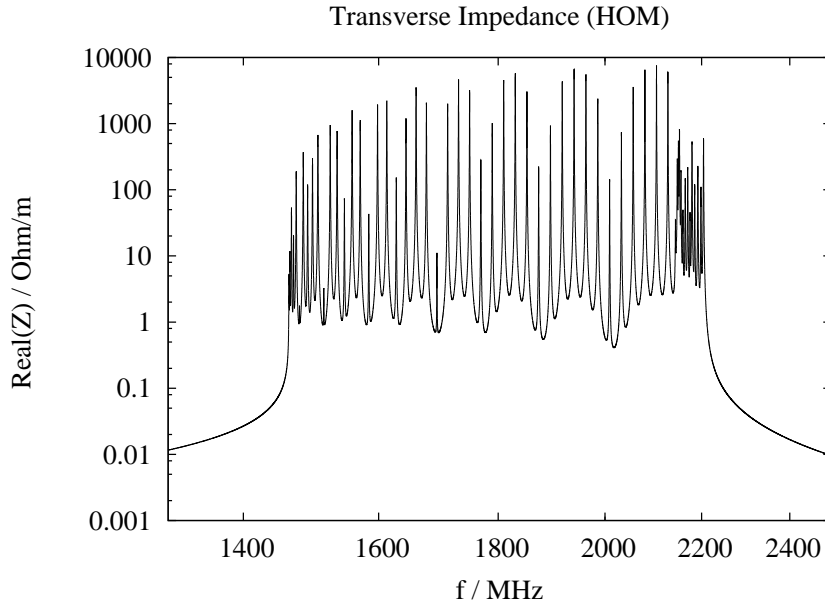


Figure 21: Real part of the transverse impedance due to HOMs using the data from Tables 8 and 9.

This is consistent with the time time domain analysis of the ATLAS vacuum chamber which showed that the longitudinal monopole and dipole impedance is almost purely inductive. The kick parameter of the ATLAS vacuum chamber without bellows is 1.72 V/pC m which is smaller than the value found for the CMS chamber of 2.38 V/pC m [2] (using a rms bunch length $\sigma_z = 7.5 \text{ cm}$). But unshielded bellows will significantly increase the transverse impedance of the ATLAS vacuum chamber. The kick parameter of *one* bellow is about 2.0 V/pC m when calculated separately from the ATLAS vacuum chamber, and there are in total ten bellows of similar type integrated in the ATLAS vacuum chamber. The transverse impedance of the chamber is therefore dominated by the unshielded bellows. It was found that a linear superposition of the results for the kick parameters is a too pessimistic model but the kick parameter of ATLAS vacuum chamber with two bellows was found to be already 4.11 V/pC m . Therefore the total kick parameter of the ATLAS vacuum chamber with ten unshielded bellows can be estimated to be about 20 V/pC m .

Acknowledgment

The research leading to these results has received funding from the European Commission under the FP7 project HiLumi LHC, GA no. 284404.

We would like to thank Elias Métral for his guidance as task leader of Task 2.4 on impedance issues and collective effects and for valuable discussion. We also thank Benoit Salvant for valuable discussion on the LHC impedance. Thanks go to Beniamino Di Girolamo and Mark Antony Gallilee who provided all the details about the ATLAS vacuum chamber which were essential for our calculations.

References

- [1] O. Brüning, H. Burkhardt, S. Myers, *The Large Hadron Collider*, Progress in Particle and Nuclear Physics, Volume 67, Issue 3, July 2012, Pages 705-734
- [2] R. Wanzenberg, O. Zagorodnova *Calculation of Wakefields and Higher Order Modes for the New Design of the Vacuum Chamber of the CMS Experiment for the HL-LHC*, CERN-ATS-Note-2013-018 TECH, CERN, April 2013
- [3] ATLAS Vacuum Layout, Drawing: LHCVC1_0001, EDMS, CERN, 2008
- [4] T. Weiland, R. Wanzenberg, *Wakefields and Impedances*, in: Joint US-CERN part. acc. school, Hilton Head Island, SC, USA, 7 - 14 Nov 1990 / Ed. by M Dienes, M Month and S Turner. - Springer, Berlin, 1992- (Lecture notes in physics ; 400) - pp.39-79.
- [5] W.K.H. Panofsky, W.A. Wenzel, *Some consideration concerning the transverse deflection of charged particles in radio-frequency fields*, Rev. Sci. Inst. Vol 27, 11 (1956), 967.
- [6] T. F. Günzel, *Transverse Coupling Impedance Of The Storage Ring At The European Synchrotron Radiation Facility*, Phys. Rev. ST Accel. Beams **9** (2006) 114402.
- [7] D.R. Lide, Ed. *Handbook of Chemistry and Physics*, 79th edition, 1998-1999, CRC Press, Washington, D.C.
- [8] P.B. Wilson *High Energy Electron Linacs: Application to Storage Ring RF Systems and Linear Colliders*, AIP Conference Proceedings 87, American Institute of Physics, New York (1982),p. 450-563.
- [9] I. Zagorodnov and T. Weiland, *TE/TM field solver for particle beam simulations without numerical Cherenkov radiation*, Phys. Rev. ST Accel. Beams **8** (2005) 042001.

- [10] I. Zagorodnov, *Indirect methods for wake potential integration*, Phys. Rev. ST Accel. Beams **9** (2006) 102002 [arXiv:physics/0606049].
- [11] A. Novokhatski and T. Weiland, *Inductive impedance and longitudinal instability*, Proceedings of the 7th European Particle Accelerator Conference (EPAC 2000), Vienna, Austria, 26-30 Jun 2000.
- [12] R. Wanzenberg, *The Impedance of Selected Components of the HERA Proton Ring*, DESY HERA 95-07, Nov. 1995
- [13] VA Aluminium Chamber Subassembly, Drawing: LHCVC1AX0002, EDMS, CERN, 2012
- [14] T. Weiland, *On the numerical solution of Maxwell's Equations and Applications in the Field of Accelerator Physics*, Part. Acc. 15 (1984), 245-292.
- [15] *MAFIA Release 4 (V4.200)* CST AG, Bad Nauheimer Str. 19, 64289 Darmstadt, Germany.
- [16] T. Weiland, *On the computation of resonant modes in cylindrically symmetric cavities*, NIM 216 (1983) 329-348.